Robotica (2005) volume 23, pp. 669–680. © 2005 Cambridge University Press
doi:10.1017/S0263574704001407 Printed in the United Kingdom

A real-time joint trajectory planner for dynamic walking bipeds in the sagittal plane

J. Vermeulen*, B. Verrelst, D. Lefeber, P. Kool and B. Vanderborght

Vrije Universiteit Brussel, Department of Mechanical Engineering, Pleinlaan 2, 1050 Brussels (Belgium)

(Received in Final Form: December 6, 2004)

SUMMARY

A real-time joint trajectory generator for planar walking bipeds is proposed. This trajectory planner generates dynamically stable motion patterns by using a set of objective locomotion parameters as its input, and by tuning and exploiting the natural upper body dynamics. The latter can be determined and manipulated by using the angular momentum equation. Basically, trajectories for hip and swing foot motion are generated, which guarantee that the objective locomotion parameters attain certain prescribed values. Additionally, the hip trajectories are slightly modified such that the upper body motion is steered naturally, meaning that it requires practically no actuation. This has the advantage that the upper body actuation hardly influences the position of the Zero Moment Point. The effectiveness of the developed strategy is demonstrated by simulation results.

KEYWORDS: Walking biped; Real-time trajectory planning; Natural dynamics; Angular momentum; Objective locomotion parameters.

I. INTRODUCTION

I.1. Real-time trajectory generation

One of the most crucial aspects of motion control for bipedal robots is the design of reference trajectories for the different joints. It is well known that arbitrarily defining those trajectories can result in all kinds of difficulties, amongst which a high energy consumption of the tracking actuators, and the possible instability of the robot caused by tipping over during the intermittent, unilateral contact phases with the supporting ground, are the most pertinent ones. Most research in this field has been done on humanoid robots, which are bipedal robots having the same locomotive structure as humans. As correctly summarized by Sugihara et al.,[1] the previous works in motion generation for humanoid robots can be classified into two main approaches, being trajectory replaying and realtime generation, or roughly speaking off-line and on-line techniques. Although the latter group is far more promising from the point of view of high-mobility and autonomy of a humanoid, most walking trajectory generation methods successfully applied today belong to the first group. In general, off-line joint trajectories are calculated in advance by using numerical optimization algorithms, or are captured from human motions, and are applied to the real robot with no or little on-line modification. The overall motion control is thus divided in two clearly distinct subproblems, being planning and control. Conversely, a real-time generation algorithm has to calculate joint trajectories in accordance with a predefined goal of the motion, while feeding back the present state of the system. Thus, planning and control form one unified task. In order to limit the number of computations, to make real-time generation possible, several authors have developed techniques based on simplification of the dynamics. During the single support phase of a walking biped, the dynamics of the system are similar to the dynamics of an inverted pendulum, whose supporting point is located at the Zero Moment Point (ZMP).[2] Using these simplified dynamics, Sugihara et al.[1] proposed a real-time trajectory generator based on a dynamical relationship between the ZMP and the global centre of gravity (COG) of the robot. Although all the inertial forces other than the gravitation were not explicitly considered in the control, their approach seemed to be effective as was verified by simulations. An interesting approach developed by Kajita et al.[3] uses the dynamics of a three-dimensional inverted pendulum whose motion is constrained onto a plane, called the Three-Dimensional Linear Inverted Pendulum Mode. A simple algorithm for walking speed generation was proposed, and tested on a 12 DOF biped robot, which successfully performed a dynamically stable walking motion. Capi et al.[4] presented a method for real-time walking gait generation based on neural networks. Energy optimal gaits similar with human motion were used to teach the neural network, such that after the learning process the human gait could be quickly generated. The type of network used was a Radial Basis Function Neural Network, which belongs in fact to a curve-fitting problem in a high-dimensional space. Recently an interesting control method based on angular momentum for a walking robot was presented by Mitobe et al.[5] The angular momentum of a walking robot was controlled through ZMP manipulation. The ZMP was considered as an actuating input of the controller, which used the angular momentum of the robot as the feedback signal to update the ZMP target position. Their method can be applied real-time, and does not require an accurate tracking of joint trajectories. They did however not cover the problem of generating feasible angular momentum trajectories which guarantee that the ZMP remains in the stability region. It is that specific task that is considered in this paper.

* Corresponding author. E-mail: Jimmy.Vermeulen@vub.ac.be

https://doi.org/10.1017/S0263574704001407 Published online by Cambridge University Press

Also outside of Japan important contributions to the subject of dynamic stability of biped robots are made. In Korea, Park and Kim[6] focused on the method of the Linear Inverted Pendulum Mode, once introduced by Kajita and Tani.[7] They found that, due to the fact that this method initially ignored mass and moment of inertia of the legs, the ZMP point significantly moved away from a presumed position when applied to a model with non-zero mass and moment of inertia. Therefore they proposed a method called the Gravity Compensated Linear Inverted Pendulum Mode,[6] which included the dynamics of the free leg motion. Using this technique, they developed an on-line trajectory generation method to increase the stability robustness of locomotion, based on the ZMP equation and the sensed information of the ZMP.[8] This strategy was further refined by Park and Cho,[9] who also expanded it for the motion during a double support phase.

I.2. Principle of developed strategy

The upper body of a biped or a humanoid robot usually contains the on-board hardware of the control system, as well as the batteries in case of electric actuation, or a pressurized vessel or a compressor in case of pneumatic actuation. Therefore the upper body is generally the robot link with the largest mass and inertia. As a consequence, keeping this body upright requires significant action of the actuators, which might cause problems concerning the position of the ZMP.[2] In this paper, a planning strategy is developed that uses the angular momentum equation to estimate the natural dynamics[10] of the upper body, or in other words, the motion of the upper body when it is unactuated. The trajectories for the leg links are then established such that this natural behaviour of the upper body approximates a given prescribed behaviour. When this desired behaviour, which will be modelled by a polynomial function, is used as a reference trajectory for the upper body actuator, then the work of this actuator is limited to overcoming the minor differences between the natural trajectory and the polynomial tracking function. The advantage of this strategy is that the resulting motion of the ZMP stays well within the boundaries of the stability region during the whole locomotion process. During the single support phase the ZMP remains in the near vicinity of the ankle joint of the supporting foot. During the double support phase the ZMP travels from the rear ankle to the front ankle joint. By using this strategy, foot rotation[11] and a possible tipping over of the robot is avoided at all times. Moreover, the resulting oscillations of the upper body are limited to small back and forth motions. Another important feature of the technique is that it generates the robot's motion based on objective locomotion parameters, as introduced by Hurmuzlu[12] and later reused by several authors.[13,14]

A planar walking biped "Lucy" has been developed by the Multibody Mechanics Research Group at the Vrije Universiteit Brussel.[15] The trajectory planner described in this paper is tested by simulation on the model of Lucy. Since its effectiveness has been verified, this strategy will be implemented on the real robot in the near future. The simulated motion of Lucy contains single as well as double support phases, while also taking the impact phase into account. The strategy developed consists of a limited number of elementary computations, which makes it useful as a real-time trajectory planner for bipeds. Note that the developed method is at this point only applied on a planar mechanism moving in the sagittal plane. This does not exclude the strategy for application on 3D models, since it has been shown for these systems that the dynamics in the sagittal plane are sufficiently decoupled from the dynamics in the frontal plane, such that their control can be treated separately.[16,17]

In section II a brief description of the simulated robot model is given. Trajectory generation for the different robot joints during a double support phase is covered in section III. For the single support phases, the trajectory generation is treated in section IV. In section V, results for a particular simulated motion are extensively reported. Finally, conclusions are drawn in section VI.

II. ROBOT MODEL

Figure 1 shows a picture of the robot Lucy, whereas Figure 2 depicts the robot geometry used for the simulations. As mentioned before, the motion of the robot is limited to the sagittal plane.

The model has two articulated legs, an upper body and two feet. For the simulations, the feet are assumed to have an ignorable inertia. The knees, hips and ankles are considered as uniaxial frictionless joints. The inertial parameters of the biped are given in Table 1 (link 4 is identical to link 2, link 5 is identical to link 1).

The length of the i-th link is l_i, its mass is m_i and the moment of inertia around its COG G_i is I_i. J_i represents the rotation axis between two connected links, which is perpendicular to the sagittal plane. The total mass of the robot is 30.5 kg. There are six actuators respectively, placed

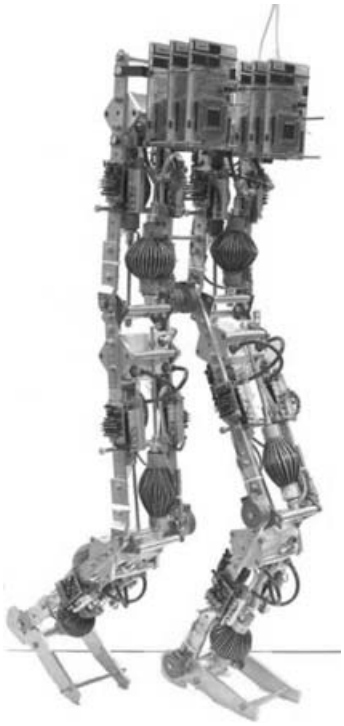


Fig. 1. Walking biped Lucy.

https://doi.org/10.1017/S0263574704001407 Published online by Cambridge University Press

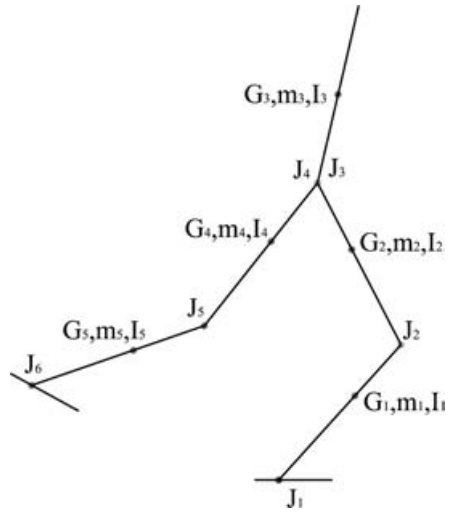


Fig. 2. Robot model.

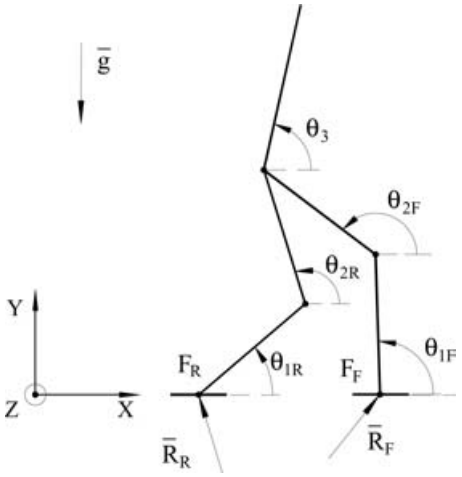


Fig. 3. Lucy during DSP.

at the hip, knee and ankle joints. A maximum five of them are used at the same time, since a foot in the air is assumed to be unactuated. In this paper, it will be assumed that whenever an actuator is not used, it does not introduce any effect of stiffness or friction on the corresponding joint. This assumption can be considered as realistic for the type of pneumatic actuators being used.[18] Note on Figure 2 that axis $J_3 = J_4$ represents the hip joint, which will further be referred to as H. Axes J_5 and J_2 are the knee joints, whereas J_1 and J_6 are the ankle joints.

III. DOUBLE SUPPORT PHASE

In Figure 3 the model of the planar biped is depicted during a double support phase. The R stands for Rear foot, whereas the F stands for Front foot.

Since both feet are in contact with the ground, a closed kinematic chain is formed by the two legs and the ground. It is desired that both feet stay in contact with the ground and that the feet do not slip during a double support phase. Due to these constraints on the feet, the robot's number of DOF is reduced to three. Indeed, during a single support phase the robot has five DOF, and during the double support phase two holonomic constraints are imposed, being:

$$X_{F_R} + l_1 \cos\theta_{1R} + l_2 \cos\theta_{2R} = X_{F_F} + l_1 \cos\theta_{1F} + l_2 \cos\theta_{2F} \tag{1}$$

$$Y_{F_R} + l_1 \sin\theta_{1R} + l_2 \sin\theta_{2R} = Y_{F_F} + l_1 \sin\theta_{1F} + l_2 \sin\theta_{2F} \tag{2}$$

The horizontal and vertical distances between the two ankle joints are respectively called step length and step height and are given by:

$$X_{F_F} - X_{F_R} = \lambda \quad \text{(step length)} \tag{3}$$

$$Y_{F_F} - Y_{F_R} = \delta \quad \text{(step heigth)} \tag{4}$$

The step length and step height belong to the set of objective locomotion parameters which form the input of the joint trajectory planner. Introducing them into the constraints leads to:

$$l_1 \cos\theta_{1R} + l_2 \cos\theta_{2R} - \lambda = l_1 \cos\theta_{1F} + l_2 \cos\theta_{2F} \tag{5}$$

$$l_1 \sin\theta_{1R} + l_2 \sin\theta_{2R} - \delta = l_1 \sin\theta_{1F} + l_2 \sin\theta_{2F} \tag{6}$$

Note that θ_3 does not appear in the holonomic constraints since the upper body is not a part of the closed kinematic chain. In the holonomic constraints, four coordinates appear, of which only two are independent. Trajectories will be established for the link angles on the rear leg by the joint trajectory planner. Calculating the values of the dependent coordinates, as well as their first and second derivatives, is straightforward.[19,20]

III.1. Hip motion during a double support phase

The following set of Lagrange's coordinates is chosen to describe the robot's motion during a double support phase:

$$q_D = \{X_H, Y_H, \theta_3\} \tag{7}$$

where X_H and Y_H, respectively, represent the horizontal and vertical position of the hip joint. A specific hip motion can be realized by tracking polynomial steer functions on the leg links of the rear leg. In order to obtain smooth trajectories, fifth order polynomials will be established. These functions connect initial and final boundary values which are deduced by the inverse kinematics applied on the following boundary values for the hip motion:

$$X_H(t_+), \dot{X}_H(t_+), \ddot{X}_H(t_+) \rightarrow X_H(t_D), \dot{X}_H(t_D), \ddot{X}_H(t_D)$$
$$Y_H(t_+), \dot{Y}_H(t_+), \ddot{Y}_H(t_+) \rightarrow Y_H(t_D), \dot{Y}_H(t_D), \ddot{Y}_H(t_D)$$

where t_+ indicates the time instance immediately after the impact phase, and t_D represents the end of the double support phase. The duration of the double support phase is then equal to $T_D = t_D - t_+$. In practice, the trajectory planner will use an inelastic impulsive impact model to calculate the joint velocity discontinuities during the shock.[21] The accelerations after the impact can be found by using the robot's equations of motion.[20] Note that if the robot starts the double support

https://doi.org/10.1017/S0263574704001407 Published online by Cambridge University Press

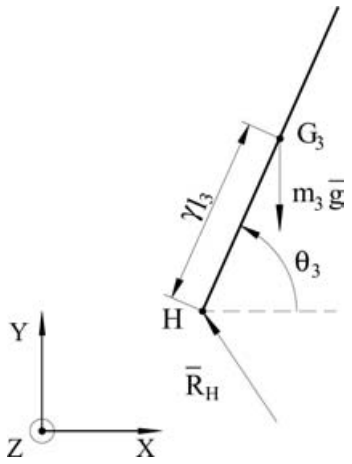


Fig. 4. FBD of upper body.

phase from rest, that $t_+ = 0$ can be chosen, combined with $\dot{X}_H(0) = 0$, $\ddot{X}_H(0) = 0$, $\dot{Y}_H(0) = 0$ and $\ddot{Y}_H(0) = 0$.

Whenever the polynomials $\theta_{1R}(t)$ and $\theta_{2R}(t)$ are known, solving equations (5) and (6) allows us to determine $\theta_{1F}(t)$ and $\theta_{2F}(t)$. These trajectories will obviously not be polynomials, and their values have to be calculated continuously by solving a quadratic equation.[20]

It is clear that, regarding the horizontal and vertical motion of the hip joint, different trajectories can be designed. During the double support phase, choosing different values for position, velocity and acceleration at $t = t_D$ results in different polynomial tracking functions. It will be shown in this work that choosing specific boundary values for the hip motion can facilitate steering the upper body motion.

III.2. Upper body motion during a double support phase

In order to derive a natural motion of the upper body during the double support phase, it is assumed that no actuator torque is acting on it. In that case, the upper body behaves as an unactuated inverted pendulum with a moving supporting point, being the hip point H. Considering the free body diagram of the upper body in Figure 4, and applying the angular momentum theorem with respect to the hip point H, yields:

$$\dot{\bar{\mu}}_H = \overline{HG}_3 \times m_3 \bar{g} + m_3 \left(\bar{v}_{G_3} \times \bar{v}_H\right) \tag{8}$$

where G_3 is the COG of the upper body and g represents gravity acceleration. Applying the transport equation for the angular momentum between H and G_3, gives:

$$\bar{\mu}_H = \bar{\mu}_{G_3} + \overline{HG}_3 \times m_3 \bar{v}_{G_3} \tag{9}$$

When differentiating with respect to time:

$$\dot{\bar{\mu}}_H = \dot{\bar{\mu}}_{G_3} + \dot{\overline{HG}}_3 \times m_3 \bar{v}_{G_3} + \overline{HG}_3 \times m_3 \bar{a}_{G_3} \tag{10}$$

Then further since

$$\dot{\overline{HG}}_3 = \bar{v}_{G_3} - \bar{v}_H \tag{11}$$

$$\dot{\bar{\mu}}_{G_3} = I_3 \ddot{\theta}_3 \bar{1}_z \tag{12}$$

Table I. Inertial parameters of the biped.

i	l_i (m)	J_iG_i (m)	m_i (kg)	I_i (kgm^2)
1	0.45	0.26	3.57	0.059
2	0.45	0.26	3.68	0.061
3	0.45	0.20	16.00	0.600

equation (8) can be rewritten as:

$$I_3 \ddot{\theta}_3 \bar{1}_z + \overline{HG}_3 \times m_3 \left(\bar{a}_{G_3} - \bar{g}\right) = 0 \tag{13}$$

This equation can be used to compute a natural motion of the upper body during the double support phase. When taking into account the following kinematic expressions (see Figure 4):

$$\overline{HG}_3 = \gamma l_3 (\cos\theta_3, \sin\theta_3) \quad \text{with} \quad \gamma = \frac{J_3G_3}{l_3} \quad \text{(see Table I)}$$

$$\bar{a}_{G_3} = \bar{a}_H + \ddot{\overline{HG}}_3$$

$$\bar{a}_H = (\ddot{X}_H, \ddot{Y}_H)$$

the following second order non-linear differential equation is found for the upper body angle θ_3:

$$\ddot{\theta}_3 = C[\ddot{X}_H \sin\theta_3 - (\ddot{Y}_H + g)\cos\theta_3] \tag{14}$$

with

$$C = \frac{m_3 \gamma l_3}{I_3 + \gamma^2 l_3^2 m_3} \tag{15}$$

One can prescribe X_H and Y_H by e.g. polynomial functions and solve this equation numerically for θ_3. Often such a problem is approached by linearizing the equation under the assumption that the rotation of the pendulum is small.[22] Here this assumption leads to:

$$\sin\theta_3 \approx 1$$

$$\cos\theta_3 \approx \frac{\pi}{2} - \theta_3$$

Such that the differential equation becomes:

$$\ddot{\theta}_3 = C\left[\ddot{X}_H - (\ddot{Y}_H + g)\left(\frac{\pi}{2} - \theta_3\right)\right] \tag{16}$$

Equation (16) clearly indicates that by varying the values of $\ddot{X}_H$ and $\ddot{Y}_H$ in the boundary points of the double support phase, different natural upper body trajectories can be obtained. When $X_H(t)$ and $Y_H(t)$ are given functions of time, and when initial conditions $\dot{\theta}_3(t_+)$ and $\theta_3(t_+)$ are specified, this equation can be numerically integrated to obtain a natural upper body motion during the double support phase. However, the goal here is not to determine a natural motion exactly, but to develop a trajectory for the upper body angle which corresponds to a motion close to a natural motion. In that case, tracking this trajectory will only demand a limited actuating torque. This implies that keeping the upper body upright will not introduce undesired motions of the ZMP.[20]

https://doi.org/10.1017/S0263574704001407 Published online by Cambridge University Press

A rough approximation of the natural upper body motion can be found by considering only the horizontal hip motion (by assuming that $\theta_3 \approx \frac{\pi}{2}$):

$$\ddot{\theta}_3^{nat} = C\ddot{X}_H \tag{17}$$

By twice integrating (17) over time, one obtains:

$$\theta_3^{nat}(t) = \theta_3(t_+) + (t - t_+)\dot{\theta}_3(t_+) + C[X_H(t) - X_H(t_+) - (t - t_+)\dot{X}_H(t_+)] \tag{18}$$

Suppose now that the duration of the double support phase is given the following value:

$$T_D = \frac{X_H(t_D) - X_H(t_+)}{\dot{X}_H(t_+)} \tag{19}$$

then roughly speaking the upper body angle at the end of the double support phase is equal to:

$$\theta_3^{nat}(t_D) = \theta_3(t_+) + T_D\dot{\theta}_3(t_+) \tag{20}$$

A fifth order polynomial function will be established for the upper body angle, connecting the following initial and final boundary values:

$$\theta_3(t_+), \dot{\theta}_3(t_+), \ddot{\theta}_3(t_+) \rightarrow \theta_3(t_D), \dot{\theta}_3(t_D), \ddot{\theta}_3(t_D)$$

with

$$\theta_3(t_D) = \theta_3^{nat}(t_D) \tag{21}$$

$$\ddot{\theta}_3(t_D) = C\left[\ddot{X}_H(t_D) - (\ddot{Y}_H(t_D) + g)\left(\frac{\pi}{2} - \theta_3^{nat}(t_D)\right)\right] \tag{22}$$

and $\dot{\theta}_3(t^+)$ as well as $\ddot{\theta}_3(t^+)$ resulting from the impact phase. A suitable value for the angular velocity $\dot{\theta}_3(t_D)$ (see (53)) will be calculated in section 4.2, where calculations for the single support phase are performed.

At this point, steer functions for all robot links are developed. In practice, the robot is overactuated during a double support phase. The load can for example be distributed over the hip and knee actuators, by using a pseudo-inverse Jacobian method.[19] The ankle actuators can then be used for an extra control loop used to regain balance in case of external disturbances. This is comparable to the so-called ankle strategy for humans.[23] Such a secondary control loop belongs however not to the scope of this paper.

III.3. Position of the ZMP during a double support phase

Figure 5 depicts the planar biped during a double support phase (note that the rear ankle point coincides with the origin of the coordinate system). The point P represents the ZMP point, located on the line connecting the two ankle points. As long as both the vertical reaction forces $R_F^y > 0$ and $R_R^y > 0$ in the absence of external ankle torques, the ZMP point will be located between the two ankle points.

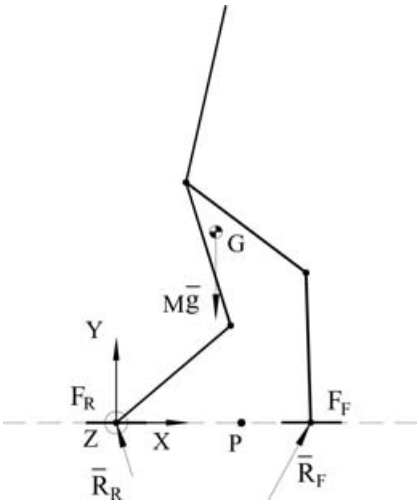


Fig. 5. Position of ZMP during a double support phase.

The position of the ZMP point can easily be calculated by applying the following definition:[24] *The ZMP point is the point where the total vertical reaction force intersects the ground*. Consequently, the moment around the ZMP caused by the vertical reaction forces in F_F and F_R has to be zero:

$$R_F^y(\lambda - OP^x) = R_R^y OP^x \tag{23}$$

Note that the distance between the two ankle points is equal to the step length λ, as defined by expression (3). The position of the ZMP is computed with:

$$OP^x = \frac{R_F^y \lambda}{R_R^y + R_F^y} \tag{24}$$

This expression states that

$$\begin{cases} R_F^y \geq 0 \\ R_R^y \geq 0 \\ R_R^y + R_F^y > 0 \end{cases} \quad \Leftrightarrow \quad 0 \leq OP^X \leq \lambda \tag{25}$$

The position of the ZMP point can also be expressed in terms of the motion of the robot instead of the ground reaction forces. Applying the angular momentum equation with respect to the rear ankle point gives:

$$\dot{\mu}_{F_R} = \overline{F_R G} \times M\bar{g} + \overline{F_R F_F} \times \bar{R}_F \tag{26}$$

from which

$$\lambda R_F^y = \dot{\mu}_{F_R} + MgX_G \tag{27}$$

Moreover, applying the linear momentum theorem in the vertical direction gives:

$$R_R^y + R_F^y = M(\ddot{Y}_G + g) \tag{28}$$

Such that the position of the ZMP is determined with:

$$OP^x = \frac{\dot{\mu}_{F_R} + MgX_G}{M(\ddot{Y}_G + g)} \tag{29}$$

https://doi.org/10.1017/S0263574704001407 Published online by Cambridge University Press

This means that in the absence of ankle torques, the trajectories for the leg links have to be defined in such a way that

$$\begin{cases} \ddot{Y}_G > -g \\ \dot{\mu}_{F_R} \geq -MgX_G \\ \dot{\mu}_{F_R} \leq -MgX_G + \lambda M(\ddot{Y}_G + g) \end{cases} \Leftrightarrow \quad 0 \leq OP^X \leq \lambda \tag{30}$$

When assuming that at the beginning of the double support phase the zero moment point coincides with the rear ankle joint, this corresponds to a zero ground reaction force at the front ankle joint. The angular momentum equation with respect to the rear ankle evaluated at $t = t_+$ then becomes (when neglecting the shift of the ZMP due to the impact):

$$\dot{\mu}_{F_R}(t_+) \approx -MgX_G(t_+) \tag{31}$$

At the end of the double support phase the zero moment point has to be located at the front ankle joint. This corresponds to a zero ground reaction force at the rear ankle joint. The angular momentum equation with respect to the rear ankle evaluated at $t = t_D$ then becomes:

$$\dot{\mu}_{F_R}(t_D) = -MgX_G(t_D) + \lambda M[\ddot{Y}_G(t_D) + g] \tag{32}$$

When designing the trajectories for the leg links in such a way that always $\ddot{Y}_G > -g$, then $\dot{\mu}_{F_R}$ increases during a double support phase. Satisfying (30) can be achieved by designing hip trajectories which do not cause $\dot{\mu}_{F_R}$ to cross the functions $-MgX_G$ and $-MgX_G + \lambda M[\ddot{Y}_G + g]$ during the double support phase.

IV. SINGLE SUPPORT PHASE

In Figure 6 the biped is depicted during a single support phase. The S stands for Supporting leg, whereas the A stands for swing (Air) leg.

Since it is assumed that the supporting foot stays in contact with the ground and does not slip during a single support phase, the number of DOF is equal to five.

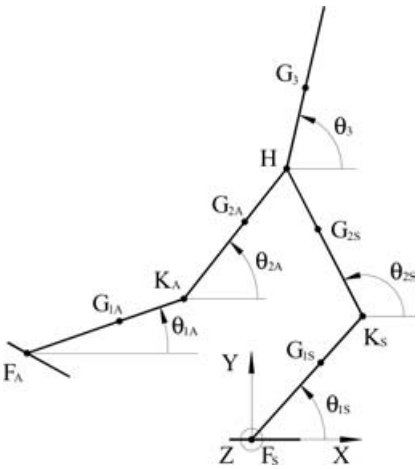


Fig. 6. Lucy during single support phase.

IV.1. Hip and swing foot motion during a single support phase

Suppose that the following set of Lagrange's coordinates is chosen to describe the motion:

$$q_S = \{X_H, Y_H, X_{F_A}, Y_{F_A}, \theta_3\} \tag{33}$$

Assuming initially that no external ankle torque is exerted, so that only the knee and hip actuators are used, the robot is an underactuated mechanism. Two fifth order polynomial functions for the leg links of the supporting leg are established, which connect the following initial and final boundary values for the hip motion:

$$X_H(t_D), \dot{X}_H(t_D), \ddot{X}_H(t_D) \rightarrow X_H(t_S), \dot{X}_H(t_S), \ddot{X}_H(t_S)$$
$$Y_H(t_D), \dot{Y}_H(t_D), \ddot{Y}_H(t_D) \rightarrow Y_H(t_S), \dot{Y}_H(t_S), \ddot{Y}_H(t_S)$$

where t_S represents the end of the single support phase. The duration of the single support phase is then equal to $T_S = t_S - t_D$. This single support phase duration is defined as:

$$T_S = \frac{X_H(t_S) - X_H(t_D)}{v} \tag{34}$$

where v is an objective locomotion parameter defining the mean horizontal hip velocity during a single support phase.

Two sixth order polynomial functions for the leg links of the swing leg are established, which connect the following initial, intermediate and final boundary values for the swing foot motion:

$$X_{F_A}(t_D), \dot{X}_{F_A}(t_D), \ddot{X}_{F_A}(t_D) \rightarrow X_{F_A}(t_i) \rightarrow X_{F_A}(t_S), \dot{X}_{F_A}(t_S), \ddot{X}_{F_A}(t_S)$$
$$Y_{F_A}(t_D), \dot{Y}_{F_A}(t_D), \ddot{Y}_{F_A}(t_D) \rightarrow Y_{F_A}(t_i) \rightarrow Y_{F_A}(t_S), \dot{Y}_{F_A}(t_S), \ddot{Y}_{F_A}(t_S)$$

The intermediate condition at $t = t_i$ is used to lift the foot whenever an obstacle has to be cleared during the swing phase. Note also that in all cases:

$$\dot{X}_{F_A}(t_D) = \ddot{X}_{F_A}(t_D) = 0 = \dot{Y}_{F_A}(t_D) = \ddot{Y}_{F_A}(t_D)$$

since during the double support phase the feet remain fixed to the ground.

IV.2. Upper body motion during a single support phase

During a single support phase, the robot rotates around the ankle point of the supporting foot F_S. The amount of rotation of the system can be quantified by the angular momentum with respect to that point. Expressing that no slip occurs and that a continuous contact of the supporting foot with the ground surface is assumed, gives:

$$\bar{v}_{F_S} = 0 \tag{35}$$

$$\bar{a}_{F_S} = 0 \tag{36}$$

where $\bar{v}_{F_S}$ and $\bar{a}_{F_S}$ are respectively the absolute velocity and acceleration of the supporting foot.

https://doi.org/10.1017/S0263574704001407 Published online by Cambridge University Press

The angular momentum can then be calculated with the general formula:

$$\bar{\mu}_{F_S} = \sum_{i=1}^{5} (\overline{F_S G_i} \times m_i \dot{\overline{F_S G_i}} + I_i \dot{\theta}_i \bar{1}_z) \tag{37}$$

thus making the sum over the 5 links. Since the motion of the robot is restricted to the sagittal plane, $\bar{\mu}_F$ is perpendicular to that plane:

$$\bar{\mu}_{F_S} = \mu_{F_S} \bar{1}_z \tag{38}$$

When expanding expression (37), the angular momentum can be written as:[20]

$$\mu_{F_S} = A_3 \dot{\theta}_3 + h \tag{39}$$

with the function h being independent of the angular velocity of the upper body $\dot{\theta}_3$. More specifically, it is calculated as follows:

$$\begin{aligned} h\bar{1}_z = {} & \overline{F_S G_{1S}} \times m_1 \dot{\overline{F_S G_{1S}}} + I_1 \dot{\theta}_{1S} \bar{1}_z + \overline{F_S G_{2S}} \times m_2 \dot{\overline{F_S G_{2S}}} \\ & + I_2 \dot{\theta}_{2S} \bar{1}_z + \overline{F_S G_{1A}} \times m_1 \dot{\overline{F_S G_{1A}}} + I_1 \dot{\theta}_{1A} \bar{1}_z \\ & + \overline{F_S G_{2A}} \times m_2 \dot{\overline{F_S G_{2A}}} + I_2 \dot{\theta}_{2A} \bar{1}_z + \overline{F_S G_3} \times m_3 \dot{\overline{F_S H}} \end{aligned} \tag{40}$$

And the function A_3 is determined by:

$$A_3 \dot{\theta}_3 \bar{1}_z = \overline{F_S G_3} \times m_3 \dot{\overline{HG}}_3 + I_3 \dot{\theta}_3 \bar{1}_z \tag{41}$$

or:

$$\begin{aligned} A_3 = {} & I_3 + m_3 \gamma^2 l_3^2 + m_3 \gamma l_3 \big[(X_H - X_{F_S}) \cos\theta_3 \\ & + \big(Y_H - Y_{F_S}\big) \sin\theta_3 \big] \end{aligned} \tag{42}$$

Taking (35) and (36) into account, one can write the angular momentum equation with respect to the ankle joint:

$$\dot{\bar{\mu}}_{F_S} = \overline{F_S G} \times M\bar{g} - \bar{T}_{F_S} \tag{43}$$

with M being the total mass of the robot and T_{F_S} the applied torque at the ankle joint of the supporting foot.

In order to obtain a natural upper body motion, it is initially assumed that the ankle actuator is not used. In that case the angular momentum equation can be written as:

$$\dot{\mu}_{F_S} = -Mg\left(X_G - X_{F_S}\right) \tag{44}$$

where X_G is the horizontal position of the global COG.

IV.2.1. Upper body angle. Integrating (44) from $u = t_D$ to $u = t$, gives:

$$\mu_{F_S}(t) - \mu_{F_S}(t_D) = -Mg \int_{t_D}^{t} \left(X_G - X_{F_S}\right) du \tag{45}$$

A second integration from $t = t_D$ to $t = t_S$ yields:

$$\int_{t_D}^{t_S} \mu_{F_S}(t)\, dt - \mu_{F_S}(t_D) T_S = -Mg \int_{t_D}^{t_S} (T_S - t)\big(X_G - X_{F_S}\big)\, dt \tag{46}$$

Now introducing (39) into the lhs of (46) and solving for $\dot{\theta}_3(t_D)$ gives:

$$\dot{\theta}_3(t_D) = F + \frac{1}{T_S A_3(t_D)} \int_{t_D}^{t_S} A_3 \dot{\theta}_3\, dt \tag{47}$$

with

$$\begin{aligned} F = \frac{1}{A_3(t_D)} \Bigg[& -Mg \int_{t_D}^{t_S} (T_S - t)\big(X_G - X_{F_S}\big)\, dt \\ & + h(t_D) T_S - \int_{t_D}^{t_S} h\, dt \Bigg] \end{aligned} \tag{48}$$

From (42) it can be seen that, when assuming small rotations of the upper body in the neighbourhood of $\frac{\pi}{2}$, as well as small vertical motions of the hip joint, the function A_3 can be approximated as a constant:

$$A_3(t) \approx I_3 + m_3 \gamma^2 l_3^2 + m_3 \gamma l_3 Y_H(t) \approx A_3(t_D) \quad (t_D \leq t \leq t_S) \tag{49}$$

Expression (47) then becomes:

$$\dot{\theta}_3(t_D) = F + \frac{\theta_3(t_S) - \theta_3(t_D)}{T_S} = F + \frac{\Delta\theta_3^S}{T_S} \tag{50}$$

Now recalling expression (20), which calculates the upper body rotation during the double support phase:

$$\Delta\theta_3^D = T_D \dot{\theta}_3(t_+) \tag{51}$$

and demanding that:

$$\Delta\theta_3^D + \Delta\theta_3^S = 0 \tag{52}$$

allows one to determine a necessary value for $\dot{\theta}_3(t_D)$:

$$\dot{\theta}_3(t_D) = F - \frac{T_D}{T_S} \dot{\theta}_3(t_+) \tag{53}$$

If this specific value for the angular velocity of the upper body is used for the construction of the polynomial function for the upper body during the preceding double support phase (see section III.2), then the upper body rotation will be compensated during the next single support phase, without requiring the use of an ankle actuator.

https://doi.org/10.1017/S0263574704001407 Published online by Cambridge University Press

IV.2.2. Upper body angular velocity. Evaluating (45) at $t = t_S$ and introducing the kinematical expression (39) yields:

$$\dot{\theta}_3(t_S) = \dot{\theta}_3(t_D) + \frac{1}{A_3(t_D)} \left[h(t_D) - h(t_S) - Mg \int_{t_D}^{t_S} \left(X_G - X_{F_S} \right) dt \right] \tag{54}$$

By varying the integral on the rhs of equation (54), different values for $\dot{\theta}_3(t_S)$ can be obtained.

In case of steady walking, for example, one can choose:

$$\int_{t_D}^{t_S} \left(X_G - X_{F_S} \right) dt = 0 \quad \Leftrightarrow \quad \dot{\theta}_3(t_S) = \dot{\theta}_3(t_D) + \frac{1}{A_3(t_D)} [h(t_D) - h(t_S)] \tag{55}$$

When considering the robot as an inverted pendulum, this case corresponds to horizontal paths of equal length behind and in front of the ankle joint. Indeed, the accelerating and decelerating effect of gravity on the COG then compensate each other.

In practice a specific value for the integral on the rhs of (54) can be attained by iteratively shifting the horizontal position of the hip point $X_H(t_D)$ at the end of the double support phase, which can be done as follows. Assuming that the COG moves with a horizontal velocity equal to the velocity of the hip, which is assumed to be constant, yields:

$$\dot{X}_G \approx \dot{X}_H \approx v \tag{56}$$

The COG then propagates with a constant speed from $X_G(t_D)$ to $X_G(t_S)$:

$$X_G(t) \approx X_G(t_D) + v T_S \tag{57}$$

so that the integral can be estimated with:

$$I = \int_{t_D}^{t_S} \left(X_G - X_{F_S} \right) dt \approx T_S \left[X_G(t_D) - X_{F_S}(t_D) + v \frac{T_S}{2} \right] \tag{58}$$

with T_S being defined by (34). The variation of I, when varying $X_G(t_D)$ and $X_G(t_S)$ in such a way that the value of T_S remains unchanged, gives:

$$\Delta I = \Delta X_G(t_D)\, T_S \tag{59}$$

which means that if a variation ΔI of the integral is desired, then the initial position of the COG has to be shifted with $\frac{\Delta I}{T_S}$.

Now assuming that

$$\Delta X_H(t_D) \approx \Delta X_G(t_D) \tag{60}$$

one obtains the following iteration formula:

$$X_H(t_D)^{,n+1} = X_H(t_D)^{,n} + \frac{\Delta I_n}{T_S} \quad \text{for} \quad n \geq 0 \tag{61}$$

with

$$\Delta I_n = I_n^{des} - I_n^{real} \tag{62}$$

When using the iterative formula (61), a specific value for $X_H(t_D)$ is determined which guarantees that during the next single support phase the integral on the rhs of (54) will attain a prescribed value. This value will consequently yield a specific value for the natural angular velocity $\dot{\theta}_3(t_S)$, which is given by expression (54). The polynomial tracking function for the upper body during the single support phase will then be constructed with this value of $\dot{\theta}_3(t_S)$.

IV.2.3. Upper body angular acceleration. Evaluating (44) at $t = t_D$ and introducing the kinematical expression (39), gives:

$$A_3(t_D)\, \ddot{\theta}_3(t_D) + \dot{A}_3(t_D)\, \dot{\theta}_3(t_D) + \dot{h}(t_D) = -Mg \left[X_G(t_D) - X_{F_S}(t_D) \right] \tag{63}$$

Note that this equation corresponds to a zero ankle torque, or in other words, to a ZMP located exactly at the ankle joint when the swing foot is lifted. This ensures a stable transition from a double to a single support phase. The angular acceleration $\ddot{\theta}_3(t_D)$ results from the polynomial function during the double support phase, and is defined by expression (22). Introducing (22) into (63), results in an equation containing $\ddot{X}_H(t_D)$ and $\ddot{Y}_H(t_D)$. The function $h(t)$ was already defined by expression (40), and it can easily be verified that this is a function of the following coordinates:

$$h = h\left(\theta_{1S}, \theta_{2S}, \theta_{1A}, \theta_{2A}, \theta_3, \dot{\theta}_{1S}, \dot{\theta}_{2S}, \dot{\theta}_{1A}, \dot{\theta}_{2A}\right) \tag{64}$$

By using the robot kinematics,[20] this function can also be written in terms of the hip and swing foot velocities:

$$h = h\left(\theta_{1S}, \theta_{2S}, \theta_{1A}, \theta_{2A}, \theta_3, \dot{X}_H, \dot{Y}_H, \dot{X}_{F_A}, \dot{Y}_{F_A}\right) \tag{65}$$

So the derivative function $\dot{h}$ will also contain the hip accelerations $\ddot{X}_H$ and $\ddot{Y}_H$. Equation (63) can thus be satisfied by choosing suitable combinations of $\ddot{X}_H(t_D)$ and $\ddot{Y}_H(t_D)$. For example, if one chooses a specific value for $\ddot{X}_H(t_D)$ (< 0), then (63) combined with (22) can be solved for $\ddot{Y}_H(t_D)$.

Goswami et al.[25] use $\dot{\mu}_G$, being the rate of change of angular momentum of the entire robot computed at its COG, as a measure of overall rotational stability. They state that whenever the ground reaction force passes through the COG, the robot is rotationally stable, since then the rate of change of angular momentum is zero and the robot does not tend to tip over:

$$\dot{\bar{\mu}}_G = 0 \quad \Leftrightarrow \quad \overline{GF}_S \times \bar{R}_{F_S} = 0 \tag{66}$$

https://doi.org/10.1017/S0263574704001407 Published online by Cambridge University Press

or

$$\dot{\bar{\mu}}_G = 0 \quad \Leftrightarrow \quad \overline{GF}_S || \bar{R}_{F_S} \tag{67}$$

with $\bar{R}_{F_S}$ being the ground reaction force acting on the supporting foot. By using this condition at the transition between a double and a single support phase, we can obtain a second equation in $\ddot{X}_H(t_D)$ and $\ddot{Y}_H(t_D)$ as follows. Applying the transport equation for the angular momentum between F_S and G, gives:

$$\bar{\mu}_{F_S} = \bar{\mu}_G + \overline{F_S G} \times M \bar{v}_G \tag{68}$$

When differentiating with respect to time:

$$\dot{\bar{\mu}}_{F_S} = \dot{\bar{\mu}}_G + \overline{F_S G} \times M \bar{a}_G \tag{69}$$

Now introducing (66), and the angular momentum equation (43) with a zero ankle torque, yields:

$$\overline{F_S G} \times M \bar{g} = \overline{F_S G} \times M \bar{a}_G \tag{70}$$

or when expanding the cross products and evaluating the equation at $t = t_D$:

$$X_G(t_D)[\ddot{Y}_G(t_D) + g] = Y_G(t_D)\ddot{X}_G(t_D) \tag{71}$$

By using the robot kinematics,[20] this equation can be written as a function of $\ddot{X}_H(t_D)$, $\ddot{Y}_H(t_D)$, and $\ddot{\theta}_3(t_D)$. So equations (63), combined with (71) and (22), allows one to determine suitable values for $\ddot{X}_H(t_D)$, $\ddot{Y}_H(t_D)$, and $\ddot{\theta}_3(t_D)$.

An analogous reasoning can be done at the end of the single support phase $t = t_S$, yielding values for $\ddot{X}_H(t_S)$, $\ddot{Y}_H(t_S)$ and $\ddot{\theta}_3(t_S)$.

IV.2.4. Tracking function. In the preceding paragraphs, the natural upper body motion was manipulated such that the upper body is steered without requiring an ankle actuator, which corresponds to a ZMP located at the ankle joint during the single support phase. In order to compensate for modelling errors and possible external disturbances, a fifth order polynomial function for the upper body angle will be established. This polynomial function is constructed with the boundary values from a natural motion, meaning that it is a reasonable approximation of the natural motion. It connects the following boundary values:

$$\theta_3(t_D), \quad \dot{\theta}_3(t_D), \quad \ddot{\theta}_3(t_D) \quad \rightarrow \quad \theta_3(t_S), \quad \dot{\theta}_3(t_S), \quad \ddot{\theta}_3(t_S)$$

Consequently, the torque exerted by the ankle actuator is low, meaning that the ZMP remains in the near vicinity of the ankle joint, which is the most dynamically stable position. Note also that due to the developed strategy during the double support phase, the ZMP automatically transfers from the rear ankle to the front ankle, without requiring external torques. Indeed, polynomial trajectories are constructed, connecting two successive single support phases, each with the ZMP located exactly at the ankle joint of its supporting foot.

V. SIMULATION

To test the effectiveness of the trajectory planner, a number of different simulations were performed.[20] The results of a steady walking pattern where Lucy walks on a stairway at a walking speed corresponding to the state-of-the-art are reported here. Note that a perfect tracking by the controllers of the different joint actuators is assumed. Since all steps are identical, only graphs for one full step are shown. The following objective parameters characterize the walking pattern and form the input for the trajectory planner:

- mean horizontal hip velocity $v = 0.5 \frac{m}{s} = 1.8 \frac{km}{h}$
- step length $\lambda = 0.3\,m$
- step height $\delta = 0.1\,m$
- foot lift $\gamma = 0.15\,m$

The total step duration is approximately 0.58 s, with a single support duration $T_S = 0.46\,s$, and a double support duration $T_D = 0.12\ s$. The single support phase covers about 80% of the total step duration, which corresponds to the case of human walking at low speeds.[26]

For the graphs in this section, the reference frame XYZ is located at the ankle joint of the supporting foot during the single support phase, and at the rear ankle joint during the double support phase, as drawn in Figures 5 and 6.

Figures 7 and 8 show, respectively, the horizontal hip position and velocity during one full step, whereas Figure 9 shows the vertical hip position. The initial horizontal hip position was determined with the iterative formula (61). For this simulation, $\dot{\theta}_3(t_S) = \dot{\theta}_3(t_D)$ was chosen in (54), which results in $X_H(t_D) - X_{F_S}(t_D) = -0.133\ m$ at the beginning of the single support phase. Note on Figure 7 that the overall

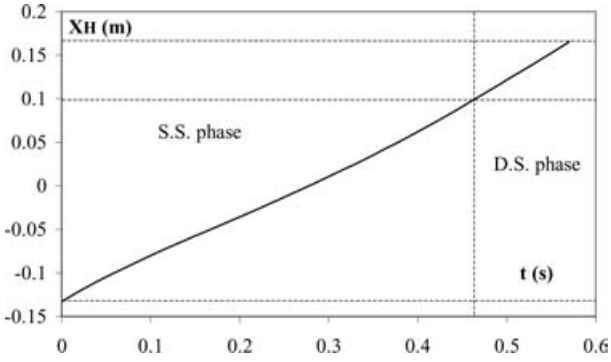


Fig. 7. Horizontal hip position.

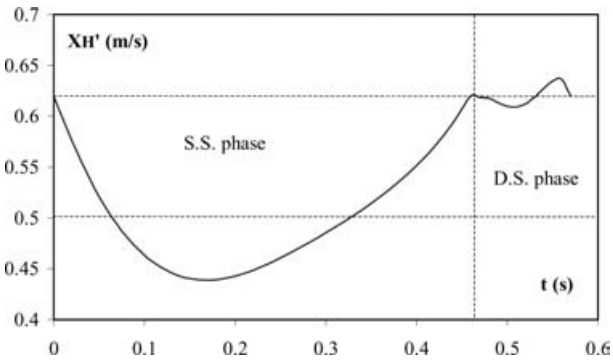


Fig. 8. Horizontal hip velocity.

https://doi.org/10.1017/S0263574704001407 Published online by Cambridge University Press

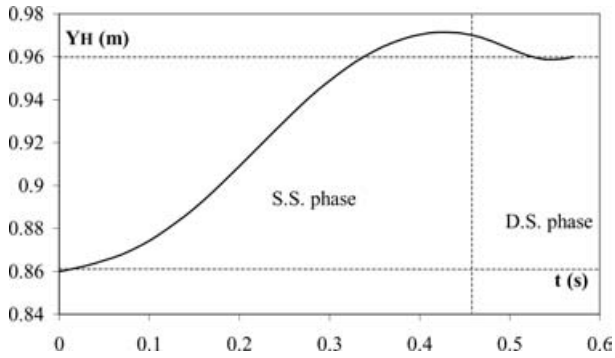


Fig. 9. Vertical hip position.

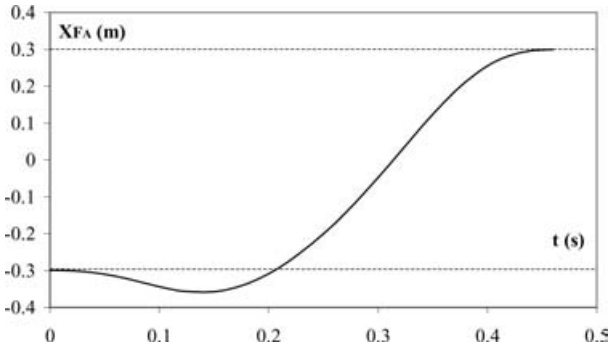


Fig. 10. Horizontal swing foot trajectory.

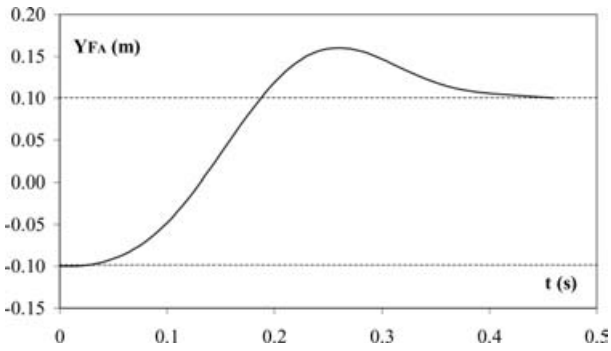


Fig. 11. Vertical swing foot trajectory.

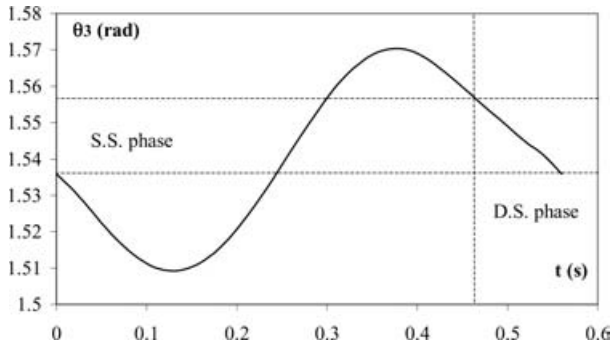


Fig. 12. Upper body angle.

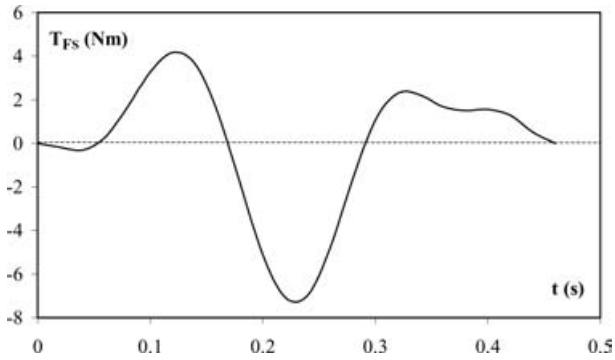


Fig. 13. Ankle torque during a SSP.

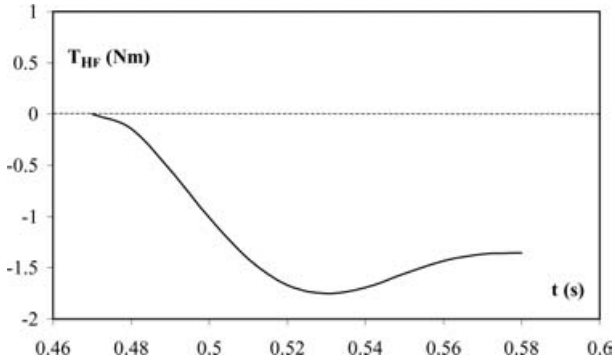


Fig. 14. Hip torque front leg during a DSP.

horizontal hip displacement equals the step length λ, which is logical for a steady walking motion. Analogously, the overall vertical hip displacement equals the step height δ, which can be verified on Figure 9. As can be seen on Figure 8, the horizontal hip velocity in the endpoints of both phases is chosen $\dot{X}_H(t_D) = \dot{X}_H(t_S) = 0.62\ \frac{m}{s}$. This corresponds to $\dot{X}_H(t_D) = \dot{X}_H(t_S) \approx 1.25\ \nu$, which appears to be interesting from the point of view of overall mechanical energy consumption.[20] Note that the bottom dashed line on this graph represents the mean horizontal hip velocity during the single support phase, which equals the prescribed value of ν. The decelerating and accelerating effect on the COG caused by gravity during the single support phase is also clearly visible on this graph.

Figures 10 and 11 show, respectively, the horizontal and vertical swing foot trajectory during a single support phase. Both the step length and the step height reach their prescribed values.

The tracking trajectories for the upper body angle during single and double support, which approximate natural trajectories, are drawn in Figure 12. It can be verified that the amplitude of the upper body oscillation is very small. For this simulation, expression (53) yields $\dot{\theta}_3(t_D) = -0.19\frac{rad}{s}$, which results in an upper body rotation $\Delta\theta_3^S = -\Delta\theta_3^D = 0.022\ rad = 1.3^\circ$ during each phase. The maximum amplitude of the upper body rotation during a full step is approximately 3.5°. Only small torques are required to actuate the upper body, as can be seen on Figures 13 and 14. Figure 13 gives the ankle torque of the supporting foot during a single support phase, whereas Figure 14 shows the hip torque on the front leg during a double support phase. Due to the fact that the trajectory generator exploits the natural upper

https://doi.org/10.1017/S0263574704001407 Published online by Cambridge University Press

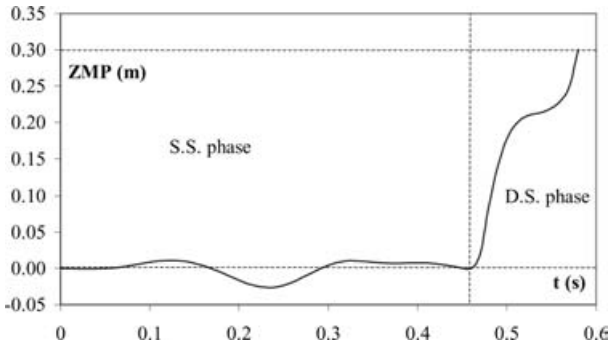


Fig. 15. Horizontal position of ZMP.

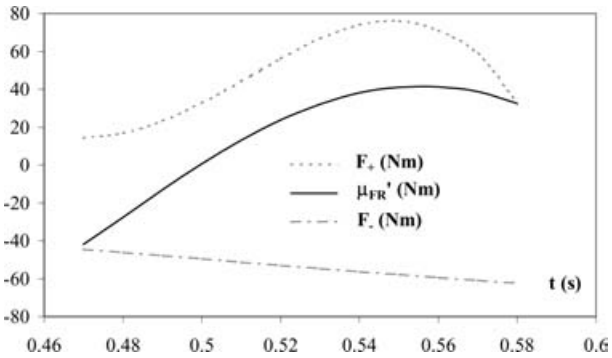


Fig. 16. Angular momentum derivative DSP.

body dynamics, the upper body actuation hardly affects the position of the ZMP.

The trajectory of the ZMP position is given in Figure 15. Indeed, during the single support phase the ZMP remains in the near vicinity of the ankle joint. During the double support phase the ZMP travels from the rear ankle to the front ankle joint. This motion of the ZMP is caused by the trajectory planner, which generates trajectories for the leg links by *a priori* taking the ZMP position into account. This is, in fact, an open-loop ZMP control strategy. During the double support phases, the trajectory generator uses the angular momentum derivative with respect to the rear ankle joint to verify that the ZMP remains between the two feet at all times. As was explained in section III.3, the value of $\dot{\mu}_{F_R}$ should never cross the functions $F_- = -MgX_G$ and $F_+ = -MgX_G + \lambda M[\ddot{Y}_G + g]$ during a double support phase. It can be seen on Figure 16 that this condition is clearly fulfilled here. This condition is easy to verify in advance since it is a purely kinematical one. As soon as the tracking functions are established, the trajectory planner checks if dynamic stability is guaranteed. If not, the hip accelerations in the boundary points are slightly adapted.[20]

Worth mentioning is that less than 20 μs of computation time was required to generate all trajectories with an AMD Athlon 1.2 GHz processor. Since only a limited number of elementary computations are made, this technique is suitable for use in real time. What particularly distinguishes the technique from other existing real-time trajectory planners, is that it does not use a simplified dynamical model. Only minor approximations are made, which has the advantage that the strategy remains effective at high walking speeds.

VI. CONCLUSIONS

A trajectory planner for the planar walking biped Lucy has been developed. A set of objective locomotion parameters form the input for this planner, while the output are polynomial tracking functions for each of the robot links. The strategy tunes the natural upper body dynamics by manipulating the angular momentum equation, so that practically no actuation is required to keep the upper body upright. As a result, external ankle torques are extremely low, which means that the upper body actuation does not cause the ZMP to move out of the stability region. The leg link angle trajectories are established in such a way that the ZMP stays in the near vicinity of the ankle joint during the single support phase, and travels from the rear to the front ankle joint during the double support phase. Since the ZMP position is taken into account when establishing the tracking functions, the trajectory planner is in fact an open loop ZMP controller. The method is very effective, as can be seen by the simulation results. Since only a limited number of computations are performed, the strategy can be used in real-time.

References

1. T. Sugihara, Y. Nakamura and H. Inoue, "Realtime humanoid motion generation through ZMP manipulation based on inverted pendulum control," *Proceedings of the 2002 IEEE International Conference on Robotics and Automation* (Washington, DC) (2002), pp. 1404–1409.
2. M. Vukobratovic and B. Borovac, "Zero-moment point – thirty five years of its life," *International Journal of Humanoid Robotics (IJHR)* **1**, No. 1, 157–173 (2004).
3. S. Kajita, F. Kanehiro, K. Kaneko, K. Fujiwara, K. Yokoi and H. Hirukawa, "A real-time pattern generator for biped walking," *Proceedings of the 2002 IEEE International Conference on Robotics and Automation* Washington, DC (2002) pp. 31–37.
4. G. Capi, Y. Nasu, L. Barolli and K. Mitobe, "Real time gait generation for autonomous humanoid robots: A case study for walking," *Robotics and Autonomous Systems* **42**, 107–116 (2003).
5. K. Mitobe, G. Capi and Y. Nasu, "A new control method for walking robots based on angular momentum," *Mechatronics* **14**, 163–174 (2004).
6. J. Park and K. Kim, "Biped robot walking using gravity-compensated inverted pendulum mode and computed torque control," *Proceedings of the 1998 IEEE International Conference on Robotics and Automation* (1998) pp. 3528–3533.
7. S. Kajita and K. Tani, "Study of dynamic biped locomotion on rugged terrain – derivation and application of the linear inverted pendulum mode," *Proceedings 1991 IEEE International Conference on Robotics and Automation*, Sacramento, California, USA (1991) pp. 1405–1411.
8. J. Park and H. Chung, "ZMP compensation by on-line trajectory generation for biped robots," *Proceedings of IEEE Conference on Systems, Man and Cybernetics (SMC'99)*, Tokyo, Japan (1999) pp. 960–965 (IV).
9. J. Park and H. Cho, "An on-line trajectory modifier for the base link of biped robots to enhance locomotion stability," *Proceedings of the 2000 IEEE International Conference on Robotics and Automation*, San Francisco, California, USA (2000) pp. 3353–3358.
10. J. Pratt, "Exploiting Inherent Robustness and Natural Dynamics in the Control of Bipedal Walking Robots," *PhD thesis* (Massachusetts Institute of Technology, 2000).
11. A. Goswami, "Postural stability of biped robots and the foot-rotation indicator (FRI) point," *Int J. Robotics Research* **18**, No. 6, 523–533 (1999).

https://doi.org/10.1017/S0263574704001407 Published online by Cambridge University Press

12. Y. Hurmuzlu, "Dynamics of bipedal gait part I: Objective functions and the contact event of a planar five-link biped," *Journal of Applied Mechanics* **60**, 331–336 (1993).
13. B. Ma and Q. Wu, "Parametric study of repeatable gait for a planar five-link biped," *Robotica* **20**, Part 3, 493–498 (2002).
14. J. Vermeulen, B. Verrelst and D. Lefeber, "Control of foot placement, forward velocity and body orientation of a one-legged hopping robot," *Robotica* **21**, Part 1, 45–57 (2003).
15. B. Verrelst, R. Van Ham, F. Daerden and D. Lefeber, "Design of a biped actuated by pleated artificial muscles," *Proceedings of the 5th International Conference on Climbing and Walking Robots (CLAWAR 2002)* (2002) pp. 211–218.
16. C. Bauby and A. Kuo, "Active control of lateral balance in human walking," *Journal of Biomechanics* **33**, 1433–1440 (2000).
17. J. Fowble and A. Kuo, "Stability and control of passive locomotion in 3D," *Proceedings of the Conference on Biomechanics and Neural Control of Movement* (1996) pp. 28–29.
18. F. Daerden, "Conception and Realization of Pleated Pneumatic Artificial Muscles and Their Use as Compliant Actuation Elements," *PhD thesis* (Vrije Universiteit Brussel, 1999).
19. C.-L. Shih and W. Gruver, "Control of a biped robot in the double-support phase," *IEEE Transactions on Systems, Man and Cybernetics* **22**, No. 4, 729–735 (1992).
20. J. Vermeulen, "Trajectory Generation for Planar Hopping and Walking Robots: An Objective Parameter and Angular Momentum Approach," *PhD thesis* (Vrije Universiteit Brussel, Belgium, 2004).
21. Y.-F. Zheng and H. Hemami, "Mathematical modeling of a robot collision with its environment," *Journal of Robotic Systems* **2**, No. 3, 289–307 (1985).
22. C.-L. Shih, "Inverted pendulum-like walking pattern of a 5-link biped robot," *Proceedings 8th International Conference on Advanced Robotics*, Monterey, California, USA (1997) pp. 83–88.
23. D. Winter, "Human balance and posture control during standing and walking," *Gait and Posture* **3**, No. 4, 193–214 (1995).
24. H. Hemami and C. Golliday Jr., "The inverted pendulum and biped stability," *Mathematical Biosciences* **34**, 95–110 (1977).
25. A. Goswami and V. Kallem, "Rate of change of angular momentum and balance maintenance of biped robots," *Proceedings ICRA '04, IEEE International Conference on Robotics and Automation*, New Orleans, USA (2004) pp. 3785–3790.
26. M. Hardt, K. Kreutz-Delgado, J. Helton and O. V. Stryk, "Obtaining minimum energy biped walking gaits with symbolic models and numerical optimal control," *Workshop – Biomechanics Meets Robotics, Modelling and Simulation of Motion*, Heidelberg, Germany (November, 1999) pp. 1–19.

https://doi.org/10.1017/S0263574704001407 Published online by Cambridge University Press